Single-electron capture by 100–1500-keV C^+ ions in several atomic and molecular targets

L. M. Rottmann, R. Bruch, and P. Neill
Department of Physics, University of Nevada, Reno, Reno, Nevada 89557-0058

C. Drexler,* R. D. DuBois, and L. H. Toburen
Pacific Northwest Laboratory, Richland, Washington 99352
(Received 5 March 1992; revised manuscript received 15 June 1992)

Experimentally determined single-electron-capture cross sections are presented for 100–1500-keV C^+ impact on He, Ne, Ar, H_2, N_2, O_2, CO, NH_3, CH_4, C_2H_6, and $(CH_3)_2$ NH gaseous targets. For the atomic targets, the single-capture cross sections were found to merge as the impact energy increased. For the molecular targets, the relative changes in the cross sections exhibit little or no dependence on the impact energy. For these systems and in the energy range considered here, the single-electron-capture cross sections were found to scale remarkably well with the "size" of the molecular target, namely with the square of the bond length for the diatomic targets and with the number of atoms comprising the polyatomic targets.

PACS number(s): 34.70.+e, 87.50.−a

I. INTRODUCTION

Electron-capture cross sections have been measured by a number of research groups. While many collision systems have been investigated over a large range of projectile energies, a wide range of collision systems that are important either for applications or for testing theoretical calculations remain largely unstudied [1,2]. Apart from the desire to develop a better understanding of the collision dynamics of charge-exchange processes, the cross-section data produced from such measurements are of vital importance in a number of fields. For example, in plasma research, contaminant carbon, nitrogen, and oxygen ions originating from various parts of the containment vessel can cool the plasma via inelastic collisions with the plasma [1]. Cross-section information for these ions is crucial in predicting plasma containment. In radiological physics, carbon, nitrogen, and oxygen recoil ions play a significant role in energy deposition in tissue during neutron exposure. These ions traverse the medium and lose energy predominantly through ionizing collisions. However, they can also capture and lose electrons in interactions with the atomic and molecular constituents of the medium. As a result of charge transfer, the number of electrons bound to the moving ion is a stochastic variable and the mean charge state is a function of the ion velocity. Since the electronic screening of the projectile charge effects the mean energy lost in ionizing collisions with the medium, changes in the charge state are reflected in the stopping power of the particle in the media. In addition, electron-capture and -loss processes contribute directly to the energy loss of charged particles.

Knowledge of absolute charge-transfer cross sections is also an important parameter in the evaluation of data obtained from ion-beam measurements, for example, determination of absolute excitation and ionization cross sections or stopping power. This is because most experiments correlate the collected ion-beam current with the number of charged particles that pass through the interaction region. Often, the experiments are conducted neglecting change in the incident-ion charge state due to interactions with the target or with background gases in the beam lines. However, when considering heavy ions at low and intermediate energy, the charge-transfer cross sections may become sufficiently large so that charge-changing interactions with the target and background gases cannot be neglected.

Generally, theoretical calculations of the charge-exchange cross sections for complex many-body systems are prohibitively difficult and, when attempted, often quite inaccurate. The theories that are available often depend on very specific conditions or they are limited to a specific collision system. For example, Firsov [3] derived the dependence of the cross section for removal of electrons as a function of the impact velocity. The formula he obtained, however, applies only to collision systems of neutral atoms or molecules. Other theories are mainly limited to fully stripped or multiply charged projectile ions or to very low or very high impact energies [4–7].

In order to supplement the available charge-transfer data, we measured the total electron-capture cross sections for C^+ ions in collisions with gaseous targets of He, Ne, Ar, N_2, O_2, CO, C_2H_6, CH_4, NH_3, and $(CH_3)_2$NH. The C^+-He data provide experimental information applicable for testing theoretical calculations for simpler target systems whereas the wide range of targets studied provides information about electron-capture systematics as a function of target parameters. In order to test for any systematic behavior as a function of the target, we have explored correlations between the cross sections and various molecular properties: the bond length of the diatomic targets, the number of scattering centers of the polyatomic targets, and the first-ionization potential of the target.

II. EXPERIMENTAL METHOD

A. General description

A schematic view of the target chamber and detection system is shown in Fig. 1. Protons and singly charged carbon ions were produced using a 2-MV Van de Graaff accelerator, were momentum analyzed, and collimated to a diameter of approximately 0.1 mm. The ions then entered a differentially pumped target cell where they interacted with a target gas. After the target cell, the ions were separated according to their charge state using an electrostatic field and counted using channel electron multipliers and standard pulse-counting techniques. A detector configuration similar to that described by Rinn *et al.* [8] was used where secondary emission resulting from the incident particle striking a stainless-steel plate is detected (see Fig. 1). The base pressure in the beam line and the target chamber was held to less than 1×10^{-6} Torr and was less than 1.5×10^{-5} Torr with target gas in the target cell.

The profile and intensity of each charge component of the beam was investigated by gradually increasing the voltage on the deflection plates and observing the count rates recorded with an off-axis detector with no gas in the target cell. A plateau was observed in the profiles which indicated that complete beam collection was achieved. Some C^{2+} contamination in the incident C^{+} beam was seen as well as some C^{0} contamination. These contaminants typically amounted to less than 5% of the total beam.

The relative detection efficiencies for the three detectors were investigated by systematically deflecting one charge-state component of the beam into different detectors and comparing the count rates. No dependence on beam energy, projectile mass, or charge state was found. The relative efficiencies, with respect to each other, were measured to be 1.0 ± 0.1. Thus the detectors were assigned unit efficiency for determination of the absolute cross sections reported here.

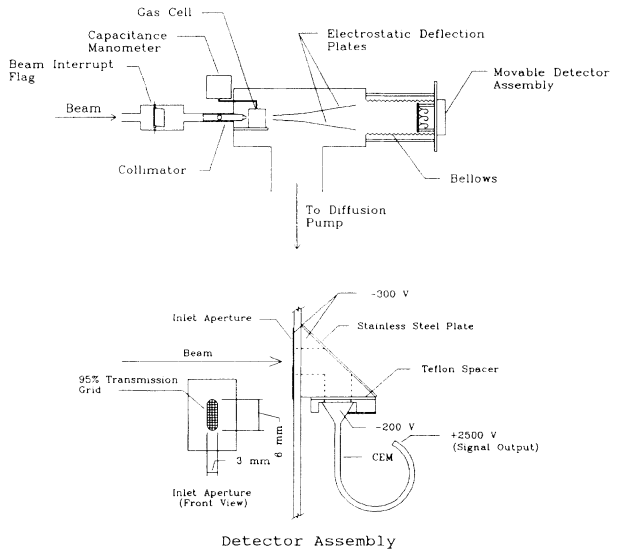

FIG. 1. Target chamber with detail of detector assembly. CEM denotes channel electron multiplier.

The target gas pressure was measured using an MKS absolute pressure manometer with a temperature-stabilized 1-Torr sensor. The diameter of the entrance aperture of the gas cell (D_1) was 0.8 mm and the diameter of the exit aperture (D_2) was 2.4 mm, the exit aperture being larger to ensure that ions undergoing small-angle scattering would be transmitted. The measured length (x) of the gas cell was 5.08 cm. To account for gas cell end effects, an effective target length x_{eff}, defined by

$$x_{\text{eff}}=x+\tfrac{1}{2}(D_1+D_2)\ , \tag{1}$$

was used in determining the absolute cross sections [9].

B. Cross-section determination

The attenuation of a beam of charged particles in charge state i interacting with a gaseous target is given by

$$\frac{dF^i}{d\pi}=\sum_{\substack{k\\k\neq i}}F^k\sigma_{ki}-F^i\sum_{\substack{j\\j\neq i}}\sigma_{ij}\ , \tag{2}$$

where F^i and F^k are the fractions of ions having charge states i and k, respectively, $(dF^i/d\pi)$ is the incremental change of ions in charge state i occurring within an increment of target density $(d\pi)$, σ_{mn} represents the cross sections for ions changing from charge state m to charge state n due to electron capture $(m>n)$ or loss $(m<n)$, and $F^i+\sum_{k(\neq i)}F^k=1$ by definition. Equation (2) is general in the sense that it allows for multiple collisions as well as effects due to contaminants in the initial beam.

In general, all possible charge states, including the possibility of multiple as well as single-electron-transfer processes, need to be considered in solving the coupled set of differential equations represented by Eq. (2). However, in the present work, many terms are small and can be neglected. For example, for incident C^{+} beams, we observed only neutral, singly charged, and doubly charged ions both before and after interactions with the target gases. Higher charge states were negligibly small. Therefore, only terms involving charge states 0, 1, and 2 need to be considered. Also, double-electron-transfer processes which would lead to charge states of -1 or $+3$ can be neglected. With these considerations, the set of equations relevant to single-electron transfer is given as follows:

$$\frac{dF^0}{d\pi}=F^1\sigma_{10}+F^2\sigma_{20}-F^0(\sigma_{01}+\sigma_{02})\ , \tag{3}$$

$$\frac{dF^1}{d\pi}=F^0\sigma_{01}+F^2\sigma_{21}-F^1(\sigma_{10}+\sigma_{12})\ , \tag{4}$$

and

$$F^0+F^1+F^2=1\ . \tag{5}$$

If it is assumed that the incoming beam is predominantly composed of singly charged ions and that single-collision conditions exist within the gas cell, for single-electron capture, the solution to Eqs. (3)–(5) becomes

$$F^0=\sigma_{10}nx_{\text{eff}}\ , \tag{6}$$

where F^0 is the neutral fraction of the emerging beam, n is the target-gas molar density, and x_{eff} is the effective gas cell length defined by Eq. (1). Single-electron-capture cross sections may therefore be obtained from the slope of the linear portion of F^0 versus the target gas pressure.

C. Data acquisition and analysis

For all measurements, the data-acquisition procedure was as follows: One detector was centered on the undeflected beam. The charge-state composition of the beam was measured by directing the charged-beam components into an off-axis detector by increasing the voltage on the beam deflectors. For C^+ beams with no gas in the target cell, impurity levels for C^0 and C^{2+} were typically measured to be less than 5% of the total beam; higher charge states were not observed. For incident protons, H^0 impurity levels comprised less than 1% of the total beam. The main source of the impurities was due to beam interactions with the collimating apertures before the target gas cell.

At each impact energy, the neutral fraction of the beam was measured as the target gas pressure was increased until the neutral component consisted of approximately 10% of the singly charged component. This ensured that the plot of the neutral fraction versus the target pressure extended well beyond the linear portion. To minimize systematic error in reading the target gas pressure, measurements were also made while decreasing the target gas pressure. From the slope of the linear portion of the curve and Eq. (6), absolute cross sections for single-electron capture were determined. At each projectile energy, measurements were made first with H_2 as the target gas, then with all the other target gases, and finally with H_2 again in order to test for any changes during the course of the measurement. Typically, the H_2 cross sections measured at the beginning and end of each set of data were reproducible to within 5%.

D. Experimental uncertainties

The overall uncertainty for the cross sections presented here comes primarily from uncertainties in the relative detection efficiencies and target gas pressure. The total uncertainties associated with the data shown in Tables I and II and in the graphical representations of the data include these uncertainties as well as uncertainties in determining the slope from F_0 versus pressure curves. An attempt was made to estimate potential errors in the measured cross sections due to beam impurities. Using our measured beam contaminant intensities and assuming σ_{01} and σ_{21} magnitudes to be twice that of σ_{10}, the effect on the measured cross sections would be a reduction of less than 10%. This is also reflected in the error bars included in the graphs of the present data.

Another potential source of error results from the possible presence of metastable ions in the incident beam. The influence of metastable ions on charge-transfer measurements has been investigated by a number of groups [10–13]. The results of these investigations seem to indicate that the effects are negligible for the energies considered in this work. We have, therefore, neglected any effects due to possible metastable component in the primary beam.

TABLE I. Measured single-electron-capture cross sections σ_{10} for C^+ on atomic and diatomic targets (in units of 10^{-16} cm^2).

Energy	Target gas					
(keV)	He	Ne	Ar	H_2	N_2	O_2
104	1.02	2.98	8.89	7.05	7.86	6.37
	±0.16	±0.46	±1.36	±1.08	±1.20	±0.97
300	1.96	2.74	4.70	3.08	4.54	4.20
	±0.30	±0.42	±0.72	±0.47	±0.69	±0.64
517	1.47	1.64	2.86	2.02	2.49	2.69
	±0.22	±0.25	±0.44	±0.31	±0.38	±0.41
1000	0.78	0.90	1.18	0.84	1.18	1.26
	±0.12	±0.14	±0.18	±0.13	±0.18	±0.19
1525	0.52	0.61	0.66	0.45	0.67	0.79
	±0.08	±0.09	±0.10	±0.07	±0.10	±0.12

TABLE II. Measured single-electron-capture cross sections σ_{10} for C^+ on polyatomic targets (in units of 10^{-16} cm^2).

Energy	Target gas				
(keV)	C_2H_6	CO	NH_3	$(CH_3)_2NH$	CH_4
104	14.9	9.20	10.5	17.8	11.1
	±2.28	±1.41	±1.61	±2.72	±1.70
300	7.52	4.59	4.85	8.98	5.65
	±1.15	±0.70	±0.74	±1.37	±0.86
517	4.68	2.82	3.25	5.77	3.67
	±0.72	±0.43	±0.50	±0.88	±0.56
1000	2.00	1.19	1.36	2.18	1.59
	±0.31	±0.18	±0.21	±0.33	±0.24
1525	1.13	0.70	0.81	1.28	0.88
	±0.17	±0.11	±0.12	±0.20	±0.13

III. EXPERIMENTAL RESULTS AND DISCUSSION

Initially, the apparatus and analysis routines were tested by comparing single-electron-capture cross sections for H^+ on N_2 and C^+ on H_2 with the recommended cross sections published by the Oak Ridge National Laboratories (ORNL) [14,15] and with the cross sections mea-

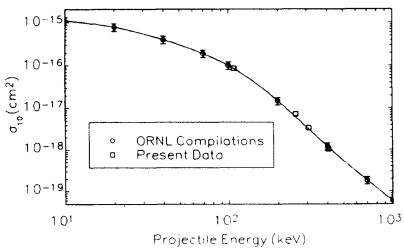

FIG. 2. Measured single-electron-capture cross sections for H^+ on N_2 compared with data from ORNL [14]. The error bars in the present data are of the size of the symbols.

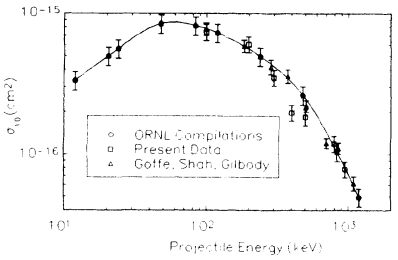

FIG. 3. Measured single-electron-capture cross sections for C^+ on H_2 compared with data from ORNL [15] and Goffe, Shah, and Gilbody [16].

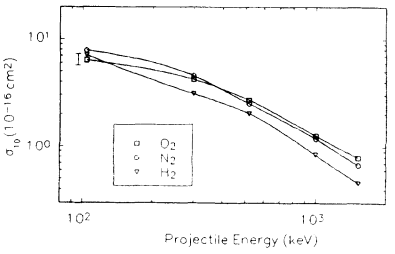

FIG. 5. Measured single-electron-capture cross sections for C^+ on diatomic targets.

sured by Goffe, Shah, and Gilbody [16]. A comparison of these data with the present measurements are shown in Figs. 2 and 3. It is evident that our present measurements are generally in good agreement with the previous measurements.

For single-electron capture by C^+ ions, our measured cross sections are presented in Figs. 4–6 and tabulated in Tables I and II. With the exception of the H_2 data discussed above, we are aware of only one reported measurement with which to compare our C^+ measurements. Hoffman, Miller, and Lockwood [17] measured single-electron-capture cross sections for low-energy C^+ ions on N_2. A portion of these data are compared with our measurements in Fig. 7. Unfortunately the two measurements overlap only for our lowest energy point and the cross section has a maximum near the point of overlap. Thus we can only comment that, although the combined results indicate that a common curve can easily be drawn through the data points, our 100-keV point is lower than theirs by approximately 24%.

The relative differences between the electron-capture cross sections for atomic targets shown in Fig. 4 are ion-velocity-dependent. As the velocity of the projectile increases above the maxima, the difference between the cross sections decreases. In the case of the molecular targets, with the exception of O_2, the relative cross sections for diatomic and polyatomic targets are velocity independent (Figs. 5 and 6). In light of this, we tested the molecular data for any empirical scaling behavior. Based on a classical description of electron capture from atomic targets, cross sections for capturing an outer-shell electron are proportional to the geometric size of the target, i.e., $\sigma \approx \pi r^2$, where r is the mean target radius. Similarly, for diatomic molecules, a potentially important parameter relating to the probability for electron capture may be the molecular-bond length since it strongly influences the target's physical size. The relationship between our measured capture cross sections for various diatomic molecules and the molecular bond lengths is shown in Fig. 8. The bond lengths were obtained from Refs. [19] and [20]. As is seen, with the exception of O_2 at the lowest ion energy, a remarkably linear relationship is exhibited. O_2 may deviate at the lowest energy because of an error in the cross section or because the O_2 cross sections exhibit a different energy dependence at lower impact energies than do the other diatomic molecules studied (see Fig. 5).

With the polyatomic targets it is more difficult to use simple bond lengths as a measure of molecular size. A more realistic picture would have to include the "shape," i.e., linear, pyramidal, etc., of the molecule and an average over its orientation in space. However, a simpler concept of the molecular size that we tested seems to provide an appropriate scaling parameter. The capture cross sections, when plotted as a function of the number of atoms comprising the target molecule, show a strong linear correlation (see Fig. 9). For the limited number of molecular targets and the projectile velocities studied here, the single-electron-capture cross sections scale according to the molecular size.

Based on work by Mapleton [18], we also investigated whether a relationship between the electron-capture cross sections and the ionization potential of the target exists. The ionization potential for the outermost electron of the molecular targets were obtained from Ref. [19]. Plots of the electron-capture cross sections as a function of the target ionization potential are shown in Fig. 10. Note that the capture cross sections decrease rapidly with in-

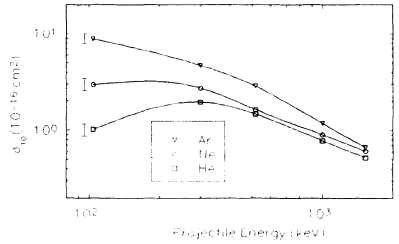

FIG. 4. Measured single-electron-capture cross sections for C^+ on closed-shell atomic targets.

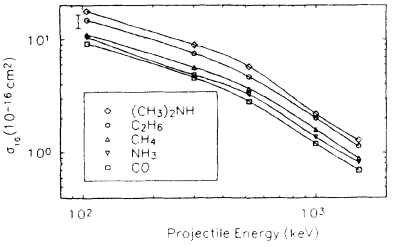

FIG. 6. Measured single-electron-capture cross sections for C^+ on polyatomic targets.

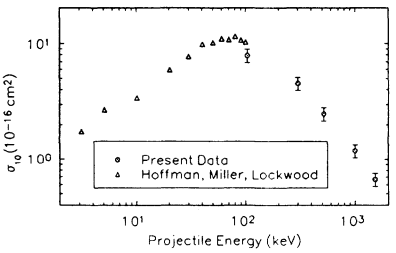

FIG. 7. Comparison of present C^+ on H_2 single-electron-capture cross sections with those measured by Hoffman, Miller, and Lockwood [17].

creasing projectile energy but that the general trend in the cross sections as a function of the target species remains the same. The data seem to group along a common curve, although cross sections for O_2, NH_3, and perhaps H_2, fall below the rest of the data. One interesting detail to be noted in Fig. 10 is that the cross section for NH_3 is consistently lower than the cross section for CH_4 even though the ionization potential is smaller for NH_3. The geometry of both CH_4 and NH_3 is that of a trigonal pyramid, although for NH_3 the trigonal pyramidal geometry arises from two unpaired electrons which distort the planar geometry. Since the two molecules have similar geometry and since NH_3 has two unpaired electrons and a smaller ionization potential than CH_4, the cross section for capturing an electron from NH_3 may be expected to be larger. The data to not support this conclusion, however. On the other hand, the bond length of

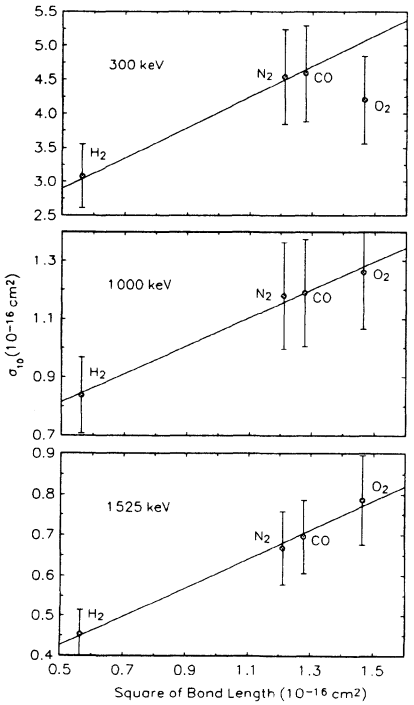

FIG. 8. Single-electron-capture cross sections as a function of the bond length for the diatomic molecules considered here [19,20].

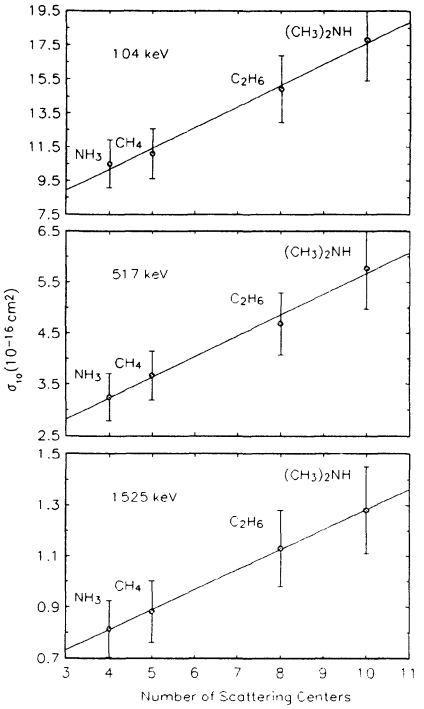

FIG. 9. Single-electron-capture cross sections as a function of the number of scattering centers of the polyatomic targets considered here.

NH_3 is smaller than that of CH_4, again supporting the idea that the molecular size is a dominating parameter in these electron-capture processes. Although we are aware of no firm theoretical basis for relating electron-capture

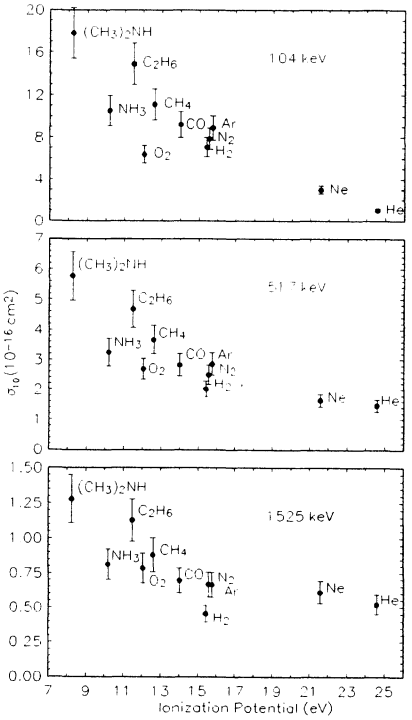

FIG. 10. Single-electron-capture cross sections as a function of the first-ionization potential of the target gas [19].

cross sections with the molecular size, Figs. 8 and 9 strongly imply that such a relationship exists.

Tests were made also of the behavior of the cross sections as a function of the number of outer-shell electrons for the target and their binding energies, but the results were generally poorer than those relating to the physical size of the targets as presented here.

IV. CONCLUSIONS

We have measured single-electron-capture cross sections for C^+ ions on several atomic, diatomic, and polyatomic targets. Our data agree well with existing data when comparisons were possible. Relationships between our measured capture cross sections and various molecular parameters such as the internuclear distance for diatomic targets, the number of atomic constituents for polyatomic targets, and the ionization potentials of the targets were investigated. Our analysis seems to indicate a strong correlation with target size and a somewhat weaker correlation with the first-ionization potential of the target. It is clear that complex collision systems such as those studied in the present work require a sophisticated model in order to better understand the dynamics involved in electron capture. Until such a model is available, the present study indicates that a simple empirical scaling of capture cross sections according to molecular "size" might be appropriate.

ACKNOWLEDGMENTS

We would like to thank Dr. Stephan Fuelling from the University of Nevada, Reno for his assistance and comments during the course of this work. We would also like to acknowledge the U.S. Department of Energy for partial support under Contract No. DE-AC06-76RLO-1830 and the Northwest Colleges and Universities for Science (NORCUS) program for support of (L.M.R.) graduate studies.

*Present address: Technical University, Munich, Germany.

[1] H. Tawara and W. Fritsch, Phys. Scr. **T28**, 58 (1989).
[2] H. B. Gilbody, A. Salin, R. Aumayr, A. Bárány, Dz. S. Belkic, F. J. de Heer, R. Hoekstra, R. K. Janev, Y. Nakai, R. D. Rivarola, H. Tawara, and T. Watanabe, Phys. Scr. **T28**, 8 (1989).
[3] O. B. Firsov, Zh. Eksp. Teor. Fiz. **36**, 1517 (1959).
[4] H. H. Fleischmann, Phys. Rev. A **5**, 1784 (1972).
[5] W. Fritsch and C. D. Lin, Phys. Rev. A **29**, 3039 (1984).
[6] W. Fritsch and C. D. Lin, J. Phys. B **17**, 3271 (1984).
[7] M. Gargaud and R. McCarroll, J. Phys. B **21**, 513 (1988).
[8] K. Rinn, A. Müller, H. Eichenauer, and E. Salzborn, Rev. Sci. Instrum. **53**, 829 (1982).
[9] R. D. DuBois and L. H. Toburen, Phys. Rev. A **31**, 3603 (1985).
[10] J. M. Hoffman, G. H. Miller, and G. J. Lockwood, Phys. Rev. A **25**, 1930 (1982).
[11] T. Kusakabe, Y. Mizumoto, K. Katsurayama, and H. Tawara, Phys. Soc. Jpn. **59**, 1987 (1990).
[12] R. A. Phaneuf, F. W. Meyer, and R. H. McKnight, Phys. Rev. A **17**, 534 (1978).
[13] Yaodong Xu, T. F. Moran, and E. W. Thomas, Phys. Rev. A **41**, 1408 (1990).
[14] Collisions of H, H_2, He, and Li Atoms and Ions With Atoms and Molecules, ORNL Report No. ORNL-6086, First Volume of ORNL-6086, 1990.
[15] Collisions of Carbon and Oxygen Ions With Electrons, H, H_2, and He, ORNL Report No. ORNL-6090, Fifth Volume of ORNL-6086, 1987.
[16] T. V. Goffe, M. B. Shah, and H. B. Gilbody, J. Phys. B **12**, 3763 (1979).
[17] J. M. Hoffman, G. H. Miller, and G. J. Lockwood, Phys. Rev. A **25**, 1930 (1982).
[18] R. A. Mapleton, Proc. Phys. Soc. **87**, 219 (1966).
[19] *CRC Handbook of Chemistry and Physics,* 65th ed. (CRC Press, Cleveland, 1984).
[20] Bernice G. Segal, *Chemistry—Experiment and Theory* (Wiley, New York, 1985).